Some Studies of Annular Extrudate Swell Phenomena

YONGSOK SEO,* *Chemical Engineering Department, University of Texas at Austin, Austin, Texas 78712*

Synopsis

As a part of continuous study, annular extrudate swell phenomena was investigated using a finite element method. For a Newtonian fluid, gravitational force and surface tension effects are considered. For non-Newtonian fluids, power-law fluid and second-order fluid were considered. Some interesting results were found for non-Newtonian fluids. For highly shear thinning fluid, thickness was contracted instead of swelling. For second-order fluid, the analysis was confined only to weak elastic fluid. Explanations are presented for high Weisenberg number problems.

INTRODUCTION

Annular die is used in many industrially important polymer processing operations, e.g., for film blowing process, blow molding process, pipe extrusion process, and hollow fiber extrusion process, to name a few. Even though it is well known that die swelling is important because it affects the final product dimension, the annular extrudate swell did not get much attention compared to capillary or planar die swelling phenomena due to its greater complexity. It is not easy to do numerical analysis for annular die swelling because it has two free surfaces of which positions are not known *a priori*. Recently there were some numerical studies about annular die swelling using a finite element method (Seo and Wissler[1,2]). In previous studies,[2] only the Newtonian fluid problem was studied. However, most of polymeric melts are non-Newtonian fluids and their behaviors are much different than a Newtonian fluids'. This article is a part of continuous study about the analysis of the annular extrudate swell problem and we investigate annular extrudate swell of non-Newtonian fluids. Also the effects of gravitational force and surface tension are considered here.

MATHEMATICAL FORMULATION AND A FINITE ELEMENT SCHEME

The mathematical description of the steady fluid motion is assumed to be given by the following equations:

$$\nabla \cdot \mathbf{v} = 0 \qquad \text{(continuity equation)} \tag{1}$$

$$\rho \mathbf{v} \cdot \nabla \mathbf{v} = \rho \mathbf{f} + \operatorname{div} \boldsymbol{\sigma} = -\nabla \mathbf{p} + \rho \mathbf{f} + \nabla \cdot \boldsymbol{\tau} \qquad \text{(momentum equation)} \tag{2}$$

*Present address: Polymer Processing Laboratory, KIST, P.O. Box 131, Cheongryang, Seoul, South Korea.

Journal of Applied Polymer Science, Vol. 41, 25–38 (1990)
 CCC 0021-8995/90/1-20025-14$04.00

Here the fluid was assumed to be incompressible. In these equations, $\mathbf{v}$ represents the fluid velocity vector, ρ the density, $\mathbf{f}$ the body force vector per unit mass, $\boldsymbol{\tau}$ deviatoric stress tensor, $\boldsymbol{\sigma}$ total stress tensor ($= -p\mathbf{I} + \boldsymbol{\tau}$), and $\mathbf{p}$ pressure.

The constitutive equation of a Newtonian fluid is presented as

$$\boldsymbol{\tau} = 2\eta_N \mathbf{D} \tag{3}$$

where $\mathbf{D}$ is the rate of strain tensor and η_N is the Newtonian viscosity. For the second-order fluid $\boldsymbol{\tau}$ is expressed as

$$\boldsymbol{\tau} = \eta \mathbf{A}^{(1)} + (\nu_1 + \nu_2)\mathbf{A}^{(1)}\mathbf{A}^{(1)} - (\nu_1/2)\mathbf{A}^{(2)} \tag{4}$$

Here ν_1 and ν_2 are material parameters called the first and second normal stress coefficients, and η is the viscosity function. The $\mathbf{A}^{(1)}$ and $\mathbf{A}^{(2)}$ are the first and second Rivlin–Ericksen tensors, respectively, defined by

$$\begin{aligned} \mathbf{A}^{(1)} &= 2\mathbf{D} = \nabla\mathbf{v} + (\nabla\mathbf{v})^T = \mathbf{L} + \mathbf{L}^T \\ \mathbf{A}^{(2)} &= \frac{\partial \mathbf{A}^{(1)}}{\partial t} + \mathbf{A}^{(1)}\mathbf{L} + \mathbf{L}^T\mathbf{A}^{(1)} + \mathbf{v} \cdot \nabla\mathbf{A}^{(1)} \end{aligned} \tag{5}$$

where $\mathbf{D}$ is the symmetric part of the velocity gradient $\mathbf{L}$ ($= \nabla\mathbf{v}$).

Substituting (5) into (4) yields the following equation for $\boldsymbol{\tau}$:

$$\begin{aligned} \boldsymbol{\tau} = {} & \eta(\mathbf{L} + \mathbf{L}^T) + (\nu_1/2 + \nu_2)(\mathbf{L}^2 + \mathbf{L}^{T2}) + (\nu_1 + \nu_2)\mathbf{L}\mathbf{L}^T \\ & + \nu_2\mathbf{L}^T\mathbf{L} - (\nu_1/2)(\mathbf{v} \cdot \nabla\mathbf{L} + \mathbf{v} \cdot \nabla\mathbf{L}^T) \end{aligned} \tag{6}$$

In eq. (6) ν_1, ν_2 and η are functions of the strain rate $\dot{\gamma}$ and temperature. Generally these can be presented as

$$\begin{aligned} \eta &= \eta_0(\dot{\gamma})^{n-1} \exp[-b(T - T_0)] \\ \nu_1 &= \nu_{10}(\dot{\gamma})^{(n_1)-1} \\ \nu_2 &= \nu_{20}(\dot{\gamma})^{(n_2)-1} \end{aligned} \tag{7}$$

Here η_0, ν_{10}, and ν_{20} are material parameters, b is a constant, T_0 is a reference temperature, and n, n_1, and n_2 are power indexes. The temperature dependence of ν_1 and ν_2 are not very well known, although they seem to depend on temperature weakly (Pipkin and Tanner[3]).

The transport of thermal energy in the fluid is described by

$$\rho C_p \mathbf{v} \cdot \nabla\mathbf{T} = \mathbf{S} + \nabla \cdot (\mathbf{k} \cdot \nabla\mathbf{T}) + \boldsymbol{\tau} : \mathbf{D} \qquad \text{(energy equation)} \tag{8}$$

where C_p is the specific heat, $\mathbf{S}$ is the volumetric heat source, and $\mathbf{k}$ is the thermal conductivity tensor. With the suitable boundary conditions, these four equations [eqs. (1), (2), (6), and (8)] form the basis of the finite element method used in this study. Using the variational statement for these equations implicitly included in conjunction with a finite element interpolation for the

independent variables **v**, p, and **T** yields the standard finite element equations. Since the finite element scheme used in this study has been fully described elsewhere,[1] we do not repeat lengthy and complicated derivation and only mention briefly the main features of this scheme. Basically the finite element method code used here is designed for steady state, incompressible, two-dimensional (plane or axisymmetric without torsion) fluid problems. It is based on the Galerkin discretization procedure, solving simultaneously eqs. (1), (2), (6), and (7) in their full nonlinear forms. Quadratic variation was used for the velocity and temperature and linear variation was used for pressure. To solve nonlinear terms, iteration was done until convergence occurs using the Newton–Raphson iteration method or the successive substitution method (Seo[4]). The computer program has been amply tested for correct simulations.

In a free surface problem, such as the die swelling problem, an additional source of nonlinearity is present since the location of the free surface is not known *a priori*. The shape of the free surface is calculated by means of an iterative procedure following those of Crochet and Keunings.[5] The other thing to be mentioned is that we can define three different swelling ratios for annular jet swelling. Those are inside diameter swelling (S_i), outside diameter swelling (S_0), and thickness swelling (S_t) as follows:

$$S_0 = \frac{\left[R_{\text{out}}^{\text{final}}(z_\infty) - R_{\text{out}}^{\text{initial}}(z_\infty)\right]}{R_{\text{out}}^{\text{initial}}(z_\infty)} = \frac{R_0^f}{R_0^i} - 1.$$

$$S_i = \frac{\left[R_{\text{in}}^{\text{initial}}(z_\infty) - R_{\text{in}}^{\text{final}}(z_\infty)\right]}{R_{\text{in}}^{\text{initial}}(z_\infty)} = 1 - \frac{R_i^f}{R_i^i} \tag{9}$$

$$S_t = \frac{\left[R_{\text{out}}^{\text{final}}(z_\infty) - R_{\text{in}}^{\text{final}}(z_\infty)\right]}{\left[R_{\text{out}}^{\text{initial}}(z_\infty) - R_{\text{in}}^{\text{initial}}(z_\infty)\right]} - 1$$

Here R_{in} means the inside radius, R_{out} the outside radius, z_∞ is far downstream, initial means the initial position before free surface iteration, and final means the final position after free surface iteration. These swelling ratios are related to each other. If R_0^i and R_i^i are 1 and k, respectively, they can be presented as follows:

$$\begin{aligned} S_0 &= R_0^f - 1 \\ S_i &= 1 - \left(R_i^f/k\right) \\ S_t &= \left(R_0^f - R_i^f\right)/(1-k) - 1 \end{aligned} \tag{10}$$

or

$$S_t = \left[(1+S_0) - (1-S_i)k\right]/(1-k) - 1$$

The problem sketch is shown in Figure 1(a) and its grid is shown in Figure 1(b). Far downstream length was varied depending on the problem. In this study, we will consider only isothermal fluids. So temperature dependency of viscosity is dropped out and energy equation (8), too.

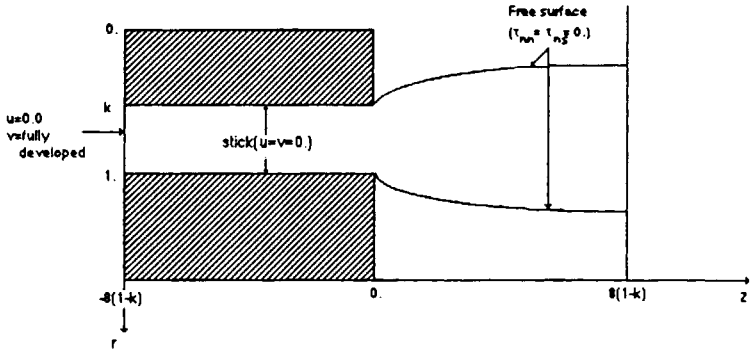

Fig. 1(a). Annular die swelling problem sketch.

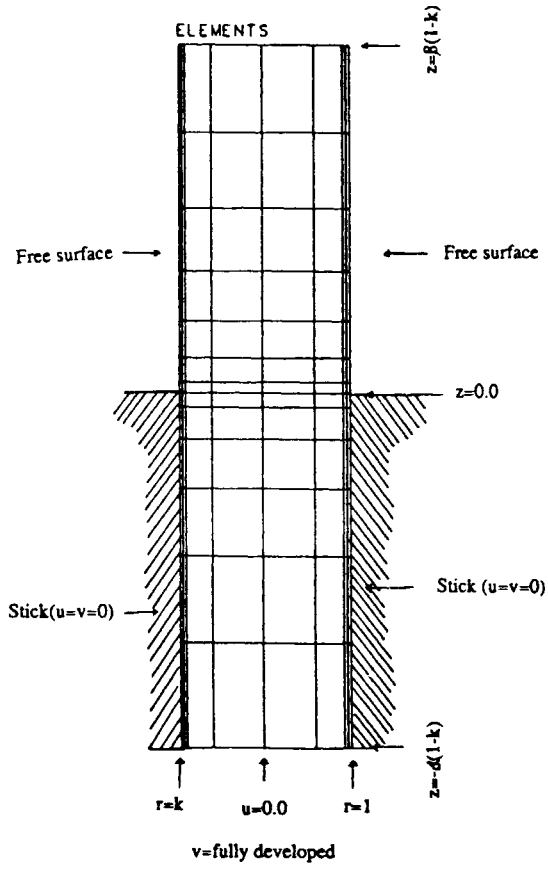

Fig. 1(b). Finite element grid for a die swelling problem.

RESULTS AND DISCUSSION

Annular Extrudate Swell with a Gravitational Force

The influence of gravitational field in determining the final shape of a creeping Newtonian fluid is now considered. Actually in the investigation of the influence of gravitational field, the overall length of the jet would be an

TABLE I
Effect of Gravity Force on the Annular Jet Swelling

g	S_0 (%)	S_i (%)	S_t (%)	FDM (S_t %)
0.0	8.6	−2.62	14.6	16.34
0.1	7.56	−2.14	13.13	15.58
0.3	6.25	−1.71	10.8	13.54
0.5	5.	−1.32	8.66	11.13
0.7	3.8	−0.98	6.66	8.97
1.0	2.21	−0.5	3.88	5.43

important factor as in extrusion blow molding process, and this has been demonstrated by the recent finite element calculations of Fischer et al.[6] However, in the present work, instead of changing far down stream domain, the gravitational parameter g was changed, where g is a dimensionless constant defined as $2g_cR/V_0^2$ (the inverse of Froude number) and g_c is the gravitational acceleration. Then gravitational force would be applied as a body force through all the region and it was taken as positive for flow direction. The meaning of this parameter g becomes clear if multiplied by Reynolds number to produce $g_cD^2V_0\rho/\mu V_0^2$, which is the ratio of gravitational force to viscous force. The same problem was solved using a finite difference method by Dutta[7] and this is the same parameter used by Dutta. An 8×13 grid was used and downstream distance was taken as four to eight times die gap. The dimensionless variables used were $R_0 = 1$, $R_i = k\ (= 0.5)$, $v_{\text{avg}} = 1$, $\rho = 1$, and $\eta = 1$. The Reynolds number was taken as 1 instead of very small value to compare with Dutta's FDM result. No slip boundary condition was applied at the die walls and normal and tangential stresses were assumed to vanish on the free surfaces. The axial direction velocity was assumed to have a fully developed profile at far upstream.

Table I demonstrates the influence of gravity in determining the shape of an annular jet emerging from a straight die. There are small differences of thickness swelling ratio from that of finite difference method result which are due to inappropriate free surface iteration of FDM (Seo and Wissler[1]). The ultimate jet shape is determined by two competing influences. One is normal stress development and another is the contraction caused by the axial force due to gravity force. We can expect that the presence of a gravitational field accelerates the fluid, increases the axial velocity, and decreases the transverse velocity and reduces the velocity gradient at die lips, which consequently tends to relieve the pressure and stress singularities at die lips (Seo[4]). It decreases swelling ratios. At far upstream in the die, the pressure is uniform because the flow is assumed a Newtonian fluid having a fully developed axial velocity profile and varies linearly with z due to the Poiseuille fluid nature of the flow. As the exit section is approached, a transverse pressure gradient develops and continues to do so until the exit plane is traversed. Beyond the exit section, this transverse gradient gradually decays and ultimately the pressure across the jet becomes uniform again. This pressure gradient and velocity redistribution after die exit causes extrudate swell (Seo and Wissler[1]). The effect of gravitational force is similar to that of pulling force acting on far downstream (Seo and Wissler[8]).

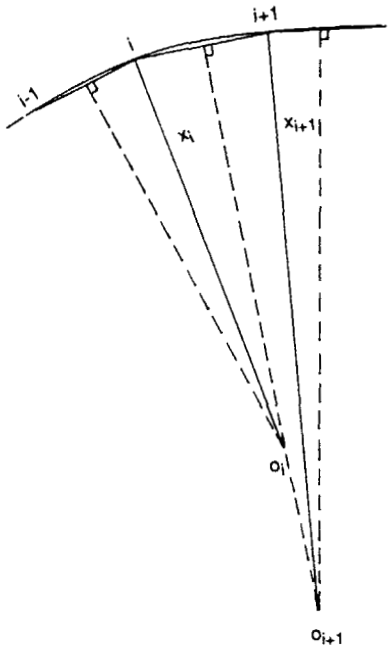

Fig. 2. Schematic figure of radius of curvature calculation.

Annular Extrudate Swell with Surface Tension

Surface tension plays an important role in determining the shape of a free surface of Newtonian fluids. For annular jets, we should consider surface tension effect on both inner and outer surfaces. This is different from the capillary flow problem which has only one free surface. For annular jets, the surface tension acts as a normal pressure on the outer surface and as a pulling force on the inner surface.

Numerical simulations incorporating surface tension involve determination of the curvature of the surface profiles. One technique, commonly used for curvature calculations is that based on spline fitting as has been suggested by Daly[9] and has been used in a modified form by Omodei[10,11] for the planar and capillary jet swelling problems. In the present study, a technique similar that employed by Reddy and Tanner[12] is adopted. The method determines the radius of curvature, X, of the surface profiles by means of purely geometrical procedure as shown schematically in Figure 2. Once X_i is evaluated at a point i on the free surface, the total curvature $1/H_i$ at the point is given by

$$1/H_i = 1/X_i + 1/\left\{R(z_i) \cdot \left[1 + (U_i/V_i)^2\right]^{0.5}\right\} \tag{11}$$

where $R(z_i)$ is the local radial position of point i and U_i and V_i are radial and axial velocity components, respectively, at point i. On the segment, $i \rightarrow i + 1$, we apply a uniformly distributed normal surface load per unit area P_i

$$P_i = \frac{\mathbf{S}^*}{2}(1/H_i + 1/H_{i+1}) \tag{12}$$

TABLE II
Effect of Surface Tension on the Annular Jet Swelling

S	S_0 (%)	S_i (%)	S_t (%)
	Re = 1		
0.0	8.37	−2.37	14.36
0.01	7.68	2.67	14.85
0.05	5.38	6.32	17.08
0.1	2.38	15.96	20.73
0.2	−3.05	37.0	30.88
0.3	−6.8	56.5	42.9
	Re = 20		
0.0	1.36	4.96	7.77
0.1	0.22	9.88	10.32

where **S** is dimensionless surface tension ($= S/\mu V_0$) which measures the ratio of surface tension to viscous forces and we make use of previous iteration geometry to evaluate the new surface loads. Now, using these values, the whole solution procedure is repeated. The process is continued until desired convergence is obtained. Downstream length was taken four to eight times the die gap. The same boundary conditions were used as before except the addition of surface tension on free surfaces. Table II summarizes the influence of surface tension on the jet swelling. As said before, the surface tension acts as a normal pressure on the outer surface and a pulling force on the inner surface. This prohibits outer surface from swelling and stimulates the inner radius swelling. The inner surface position moves more than the outside surface because the same surface tension value was applied on both surfaces and the smaller radius of curvature at inside enables a larger pulling force to act on the inner surface which pulls in the inner surface more and makes the thickness swelling ratio increase with surface tension. Figures 3 and 4 show the effect of surface tension on the shape of an annular jet when the Reynolds number is 1 and 20, respectively, for different values of the surface tension

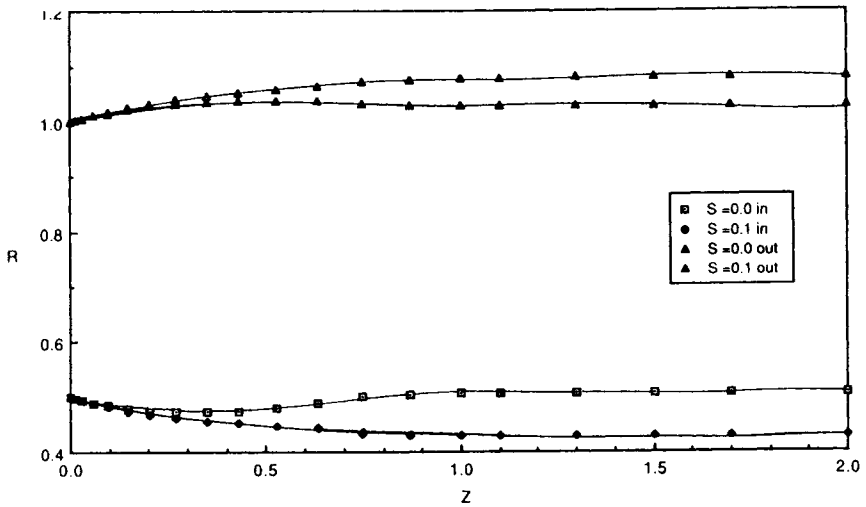

Fig. 3. Surface tension effect on the jet shape when Re = 1.

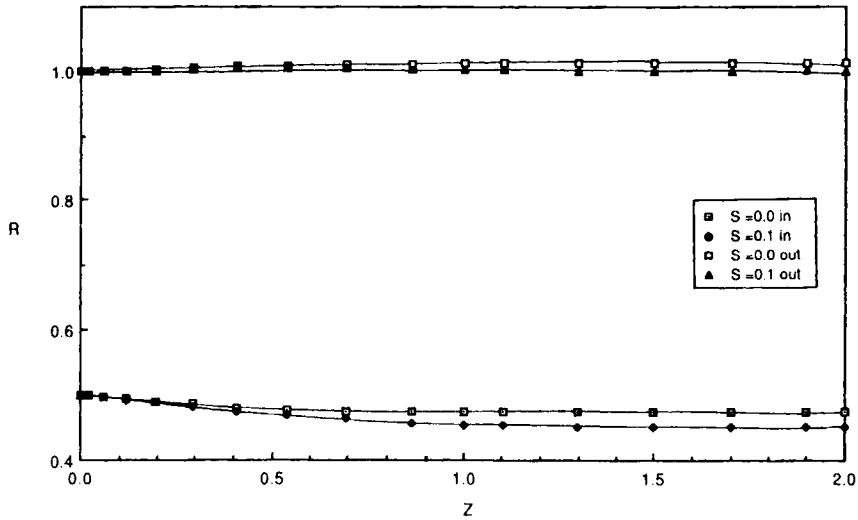

Fig. 4. Surface tension effect on the jet shape when Re = 20.

parameter **S**. From these figures we can see that when the Reynolds number is small surface tension has a considerable effect on jet shape, but when the Reynolds number becomes large, its effect decreases since the inertia is the major controlling factor for jet swelling. This is similar to Reddy and Tanner's[12] computational result for capillary jet problem. It was also observed that when **S** is small, the shape of the profile converges very rapidly to its final position. However, when **S** is large, the behavior of the free surface needs a longer domain to get a converged position at far downstream. Generally the surface tension of polymeric fluids or polymer melts is very small and the value of **S** of those are much smaller than used here. So it seems the surface tension does not affect seriously polymer melt extrusion.

Annular Extrudate Swell of Inelastic Fluids

Before studying viscoelastic fluid behavior, an inelastic non-Newtonian fluid swelling problem was considered first. The fluid referred to as "power law" fluid was used, which has a simple form of constitutive equation but is important in many industrial polymer processing operations. For simple shearing motion, the viscosity depends on shear rate nonlinearly and is presented as [written in eq. (7)]

$$\eta = \eta_0 |\dot{\gamma}|^{n-1} \tag{13}$$

where η_0 is a consistency parameter and n is the flow index. When $n = 1$, we recover a Newtonian fluid behavior and when $n < 1$, the flow is pseudoplastic (or shear thinning) and when $n > 1$, it is dilatent (or shear thickening). As explained by Tanner et al.,[13] stability consideration forbids a negative value of n, because the shear stress should not decrease with increasing shear rate. So $n = 0$ represents the lower limit for n. In this case ($n = 0$), we have a slug (or plug) flow in a die.

The computations were done using the same grid that was used for the Newtonian fluid case for $k = 0.5$ (8×13 mesh). Dimensionless variables used were $R_0 = 1$, $R_i = k$ ($= 0.5$), $v_{avg} = 1$, $\rho = 1.E - 5$, and $\eta = 1$.

The upstream and downstream length was taken eight times of die gap to get a converged shape and exclude die exit disturbances. Nine node Lagrangian elements were used. Boundary conditions on the free surfaces and solid walls are identical for previous fluids—we assume the normal and tangential stress vanish on the free surfaces and the fluid sticks to solid walls. One thing that should be mentioned is that the entry boundary condition at far upstream is more complex than for Newtonian fluid. The annular velocity profiles of a power law fluid is more difficult to obtain as shown in a paper by Fredrickson and Bird.[14] It is easy to show that the shear stress component τ_{rz} has the general form $Ar + B/r$; thus for a fluid with power law index n, we should get

$$\eta_0 |\dot{\gamma}|^n = \pm (Ar + B/r) \tag{14}$$

This equation can be solved separately for two ranges, $\dot{\gamma} \leq 0$ and $\dot{\gamma} \geq 0$, to obtain solutions that join at some radius λ, where $A\lambda + B/\lambda = 0$. A, B, and two integration constants can be obtained by specifying the flow rate, no-slip conditions at the walls, and continuity of velocity at $r = \lambda$. However, this requires considerable computational work. As an alteration, boundary condition and flow rate of a Newtonian fluid were applied at far upstream of the die; then the fluid will have a non-Newtonian fluid velocity profile marching through the fluid path. So it is necessary to use a longer domain than for a Newtonian fluid to give enough space to develop a non-Newtonian velocity profile. It was observed from numerical result that eight times length of die gap was enough for power law fluid case. The viscoelastic fluid needs a longer domain than this.

Dimensional analysis shows without gravity and negligible surface tension, the isothermal extrudate swell is a function of power-law index, n, in the creeping flow limit. Table III presents computed results for this case when Re = $1.E - 5$. The thickness swells more with increasing n. We can expect this easily considering the shearing in a die and the velocity arrangement at downstream (Seo and Wissler[1]). The fluid moves outward more with shear thickening fluid. The thickness swell is presented in Figure 5 vs. power law index n. From Figure 5 we can see that the thickness swelling ratio increases

TABLE III
Annular Jet Swelling with Power-Law Index

n	S_0 (%)	S_i (%)	S_t (%)
1.4	16.21	−9.164	23.25
1.2	12.22	−5.242	19.19
1.0	8.6	−2.6	14.6
0.8	5.38	−0.28	10.47
0.6	2.73	0.363	5.813
0.4	0.676	−0.218	1.103
0.3	−0.13	−0.845	−1.103
0.2	−0.755	−1.767	−3.277

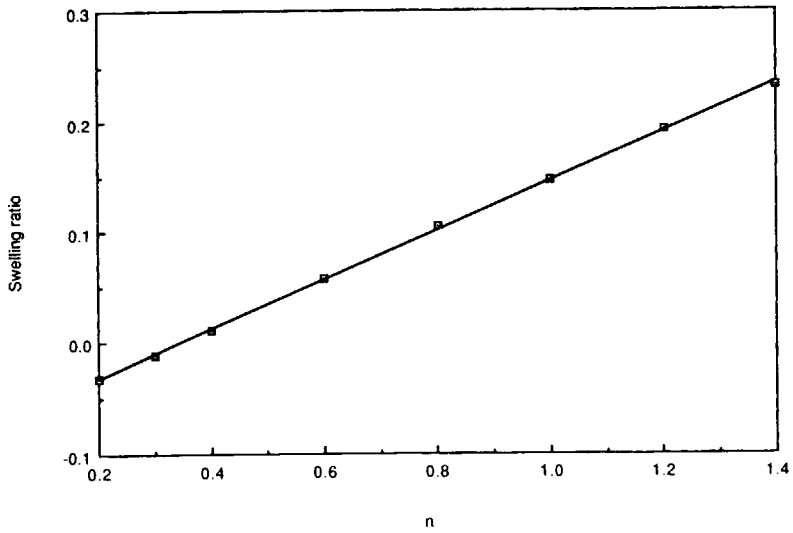

Fig. 5. Thickness swelling ratio vs. power-law index.

almost linearly when n is greater than 0.1. Also a linearized approximation line is presented in Figure 5. It is presented as

$$S_t = 0.223n - 0.077 \tag{15}$$

When n is 1.4, S_t reaches as much as 23.25%. So for a shear thickening fluid, we can expect a relatively large thickness swelling, although it is still not comparable to real polymeric fluid thickness swelling ratio. Overall thickness swelling behavior is similar to that of capillary die swelling (Huynh[15]). However, for shear thinning fluid ($n < 1$) the thickness swelling is not so large and it agrees with the well known fact that since most polymeric fluid or melts have a value of n between 0.4 and 0.6, inelastic behavior of polymeric melt or fluid is not the cause of their large extrudate swell. It should be pointed out that when the power law index is less than 0.4 in Table I, the thickness swelling ratio becomes negative, which means the thickness contracts rather than swells.

Tanner and his co-workers[13] noted that die swelling for capillary flow decreases with decreasing power law index and no swelling occurs when power law index has its minimum value, i.e., zero. The more the fluid becomes shear thinning (in other words the smaller the n value becomes), the more its axial velocity profile becomes flat in the die, but never totally flat because the stick boundary condition at the die walls requires zero velocity there. If the fluid is totally inviscid, then it is the same as when fluid flowing inside of the die slips completely, which yields a plug flow. This case was studied by Silliman and Scriven,[16] and, as we expect, admitting perfect slip (a plug flow) does not produce any swelling at all. For very small values of n, however, shearing is confined to regions near the wall and a large portion of the fluid has a higher velocity than the average axial velocity. Hence, the fluid element does not deform much after emerging from a die. This can be explained in terms of velocity changes after die exit. The axial velocity does not change

much after extrusion except near die lips. Fluid elements near die lips are under a pulling force, and elements near the fluid center are under compression to balance it. But, owing to the almost flat velocity profile in the fluid, the compression is distributed evenly across the fluid thickness. Hence, there is not large pushing from fluid center. Even though the pushing from the center is small, the stretching at die lips would be relatively large compared to compression at the center (Seo and Wissler[1]). This makes the fluid contract after extrusion. When n is less than 0.1, it took very long computational time to get a converged solution.

Annular Extrudate Swell of Viscoelastic Fluids

Needless to say, most polymeric fluids are viscoelastic fluids which is believed to be the main cause of large die swelling. When a polymeric melt enters into the die from the reservoir or extruder, the constituent molecules are entangled. While it passes through the die, its elastic strain energy is imparted to the fluid. After it leaves the die, some of the strain energy will be recovered and this elastic strain recovery causes a large thickness swelling.

As presented in eq. (7), it is possible to use parameters dependent on the second invariant of the rate of deformation tensor. However, there is a lack of data for the parameter's power-law indexes. So instead of it, we would rather use constant parameters for η, ν_1, ν_2. Upstream length was increased to $z = -12$ to get a uniform pressure profile across the die gap, since a Poiseuille flow was specified at far upstream and the far downstream length was increased to $z = 6$ to get a uniform axial velocity. The boundary conditions are the same as the power-law fluid case, where a Newtonian fully developed axial velocity profile was also specified at the upstream boundary.

For the second-order fluid, dimensional analysis provides two dimensionless variables

$$S_{\text{swelling}} = S(\nu_2/\nu_1, \nu_1 V_0/\eta R_0)$$

If we note that ν_1/η has the dimension of time, then the second-order fluid model is apparently equivalent to Maxwell fluid model as verified by Tanner.[17] In a simple shearing flow (where the velocity field is given by $\mathbf{v} = \mathbf{i}\dot{\gamma}y$) we can define the first normal stress difference N_1 by $\tau_{11} - \tau_{22}$, equal to $\nu_1\dot{\gamma}^2$, and the second normal stress difference N_2 by $\tau_{22} - \tau_{33}$, equal to $\nu_2\dot{\gamma}^2$. Hence, the first normal stress difference N_1 is proportional to $\nu_1(V_0/R_0)^2$, and it can be seen easily that the dimensionless group $\nu_1 V_0/\eta R_0$ is proportional to $(N_1/\tau_{12})_{\text{wall}}$ evaluated at the die wall; thus the equivalence of the present formulation to those based on recoverable shear $(N_1/2\tau_{12})_{\text{wall}}$ can be easily understood (Tanner[18]). The dimensionless number $\nu_1 V_0/\eta R_0$ is generally called the Weisenberg number, which is a measure of the relative importance of elastic effects to viscous effects. The starting dimensionless values of the material parameters used in this problem were $\eta = 1$, $\nu_1 = 0.1$, and $\nu_2 = -0.01$. The first normal stress difference coefficient ν_1 was varied to change the Weisenberg number while all other variables were kept fixed. The computational result is presented in Table IV for a limited range of Weisenberg number (We), which is based on annular die gap (0.5). When the Weisenberg number is larger than 0.4, 20 iterations were not enough to get a converged

TABLE IV
Summary of Annular Jet Swelling for a Second-Order Fluid

We	S_0 (%)	S_i (%)	S_t (%)
0.1	10.52	−0.27	20.79
0.2	12.28	1.01	25.57
0.3	14.61	1.77	30.99
0.4	17.78	1.39	37.35

solution. Additional iteration costs a lot of computational time. In the limited range of We for which solutions were obtained, we can get a glimpse of the elastic effect on annular jet swelling. Table IV shows that increasing We gives large thickness swelling, as we would expect. It is reported by others (Chang et al.,[19] Tanner,[17] and Murty[20]) that when the We increases, thickness swelling of a capillary jet decreases first and then increases. This slacking phenomenon with increasing We was not found in our result, possibly due to coarse mesh.

Figures 6(a) and (b) show the axial stress contours for the We = 0 (Newtonian fluid) and We = 0.4 cases. In these figures, due to the magnification of radial direction, the annular jet shapes are exaggerated in the radial direction. However, we can see clearly the axial stress develops with non-Newtonian fluid and very high extensional stresses arise at the die lip with increasing We. In our computational results, it was found that the radial stress increased at the lips, while the pressure singularity at the lips lost its intensity when We increased (Seo[4]). It is a possible conjecture that these high extensional stresses are causing the eventual lack of convergence of the numerical procedure.[21] Recently a lot of progress has been made to solve the high Weisenberg number problem and it was revealed that the traditional Galerkin

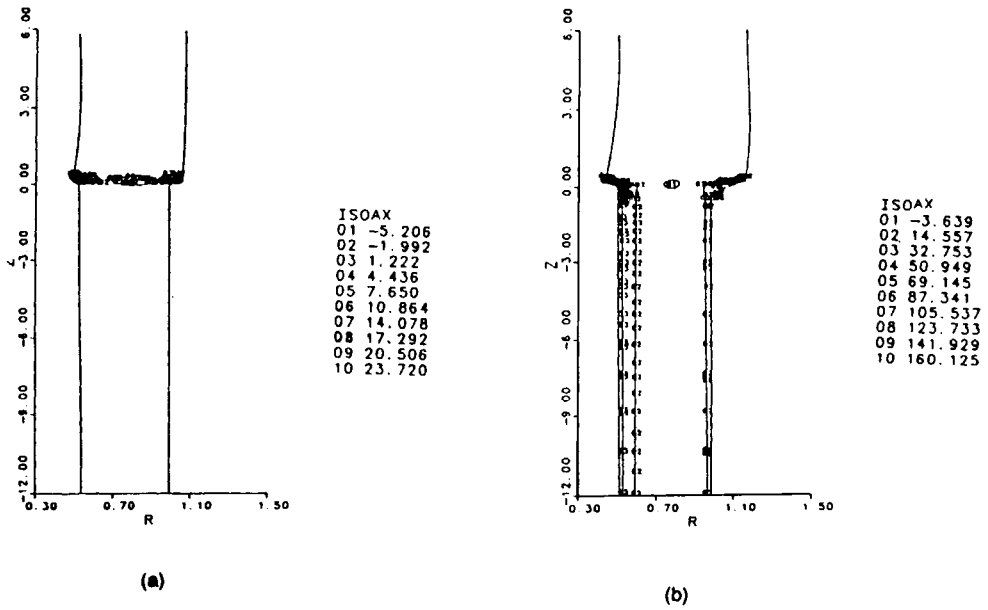

Fig. 6. Axial stress fields for (a) Newtonian fluid and (b) second order fluid.

TABLE V
The Effect of the Second Normal Stress Difference Coefficient on Annular Die Swelling When $\nu_1 = 0.1$

ABS (ν_2/ν_1)	S_0 (%)	S_i (%)	S_i (%)
0.1	10.52	−0.27	20.79
0.2	10.0	0.3	20.30
0.3	9.5	0.82	19.84
0.4	9.02	1.3	19.35
0.5	8.56	1.74	18.85

method cannot overcome the bifurcation point of highly elastic fluid (Keunings[22]). Also second order fluid model was found to be an inappropriate constitutive equation to solve high Weisenberg number problem (Luo and Tanner[23]). This is a quite active area and further study is under way.

From dimensional analysis we have another dimensionless coefficient ν_2/ν_1. The second normal stress difference coefficient is probably an order of magnitude smaller than the first normal stress difference coefficient and its sign is opposite to the first normal stress difference coefficient (Bird et al.[24]). It is known that the second normal stress difference is responsible for the larger pressure at the inner cylinder for axial annulus flow even if the pressure difference is not large (Tadmor and Gogos[25]). This agrees with the computational result presented in Table V. The larger the absolute value of ν_2, the more fluid moves inward and radius swelling increases. Also we can see that thickness swelling does not change appreciably even though the absolute value of ν_2/ν_1 was changed as much as five times. For polymeric fluids, the absolute value of ν_2/ν_1 is believed to lie between 0.1 and 0.3. So it seems that the influence of the second normal stress difference is not so significant as that of the first normal stress difference coefficient. This confirms Tanner's assumption[18] that the effect of the second normal stress difference on die swelling is not large.

CONCLUSIONS

In this paper annular die swell was studied. The effect of gravitational force was similar to that of pulling force acting on far downstream (Seo and Wissler[8]). Increasing gravity force reduces the compression on the fluid center at die exit position and reduces swelling ratios. Surface tension effect on annular extrudate swell showed larger inner radius and thickness swelling ratios and reduced outer radius swelling ratio. Surface tension effect does not seem so important in real polymer processing due to small value. For the non-Newtonian fluid constitutive equation, the power-law model and second-order fluid model were used. Inelastic viscous fluid (power-law fluid) showed increasing swelling ratios with the power-law index. In other words, the shear thickening fluid got more swelling, but, as well known, the swelling ratios are not so large even for very shear thickening fluid. For the second-order fluid case, the converged solution could be found for only the weak elastic fluid and the computation met the so-called high Weisenberg number limit. Within a

converged solution range, slacking phenomenon with increasing Weisenberg number was not observed. To be more useful, numerical analysis should be able to overcome this barrier and recent studies illuminate some lights in this area. This study will be continued in the future. The influence of the second normal stress difference coefficient does not seem to be significant and this numerical result supports Tanner's assumption.

References

1. Y. Seo and E. H. Wissler, *J. Appl. Polym. Sci.*, (1988), **37**, 1159 (1989).
2. Y. Seo, Polym. Eng. Sci., **30**, 235 (1990).
3. A. C. Pipkin and R. I. Tanner, *Mech. Today*, **1**, (1972).
4. Y. Seo, Ph.D. dissertation, University of Texas at Austin, 1987.
5. M. J. Crochet and R. Keunings, *J. Non-Newtonian Fluid Mech.*, **7**, 199 (1980).
6. R. J. Fischer, M. Denn, and R. I. Tanner, *Ind. Eng. Chem. Fundam.*, **19**, 195 (1980).
7. A. Dutta, Ph.D. thesis, State University of New York at Buffalo, 1981.
8. Y. Seo and E. H. Wissler, *Polym. Eng. Sci.*, **29**, 722 (1989).
9. B. J. Daly, *J. Comput. Phys.*, **4**, 97 (1969).
10. B. J. Omodei, *Comput. Fluids*, **7**, 179 (1979).
11. B. J. Omodei, *Comput. Fluids*, **8**, 275 (1980).
12. K. R. Reddy and R. I. Tanner, *J. Rheol.*, **22**, (1978).
13. R. I. Ranner, R. E. Nickel, and R. W. Bilger, *Comput. Methods Appl. Mech. Eng.*, **6**, 15 (1980).
14. A. G. Fredrickson and R. B. Bird, *Ind. Eng. Chem.*, **50**, 347 (1958).
15. B. P. Huynh, *J. Non-Newtonian Fluid Mech.*, **13**, 1 (1982).
16. W. J. Silliman and L. E. Scriven, *J. Comput. Phys.*, **34**, 287 (1980).
17. R. I. Tanner, *J. Non-Newtonian Fluid Mech.*, **7**, 265 (1980).
18. R. I. Tanner, *J. Polym. Sci. A-2*, **18**, 2067 (1970).
19. P. W. Chang, T. W. Pattern, and B. A. Finlayson, *Comput. Fluid.*, **7**, 285 (1979).
20. V. D. Murty, Ph.D. dissertation, University of Texas at Austin, 1982.
21. J. M. Marchal and M. J. Crochet, *J. Non-Newtonian Fluid Mech.*, **26**, 77 (1987).
22. R. Keunings, *J. Non-Newtonian Fluid Mech.*, **20**, 269 (1986).
23. X. Luo and R. I. Tanner, *J. Non-Newtonian Fluid Mech.*, **22**, 61 (1987).
24. R. B. Bird, R. C. Armstrong, and O. Hassager, *Dynamics of Polymeric Liquids*, Wiley, New York, 1977, Vol. 1.
25. Z. Tadmor and C. Gogos, *Principles of Polymer Processing*, Wiley, New York, 1979.

Received May 18, 1988
Accepted December 12, 1988